Published in final edited form as:

ACS Nano. 2017 July 25; 11(7): 7091–7100. doi:10.1021/acsnano.7b02718.

Nanopore Sensing of Protein Folding

Wei Si[†,‡] and **Aleksei Aksimentiev**[*,†]

[†]Department of Physics, University of Illinois at Urbana-Champaign, Urbana, Illinois 61801, United States

[‡]Jiangsu Key Laboratory for Design and Manufacture of Micro-Nano Biomedical Instruments and School of Mechanical Engineering, Southeast University, Nanjing, 210096, China

Abstract

Single molecule studies of protein folding hold keys to unveiling protein folding pathways and elusive intermediate folding states—attractive pharmaceutical targets. Although conventional single-molecule approaches can detect folding intermediates, they presently lack throughput and require elaborate labeling. Here, we theoretically show that measurements of ionic current through a nanopore containing a protein can report on the protein's folding state. Our all-atom molecular dynamics simulations show that the unfolding of a protein lowers the nanopore ionic current, an effect that originates from the reduction of ion mobility in proximity to a protein. Using a theoretical model, we show that the average change in ionic current produced by a folding-unfolding transition is detectable despite the orientational and conformational heterogeneity of the folded and unfolded states. By analyzing millisecond-long all-atom MD simulations of multiple protein transitions, we show that a nanopore ionic current recording can detect folding-unfolding transitions in real time and report on the structure of folding intermediates.

Graphical Abstract

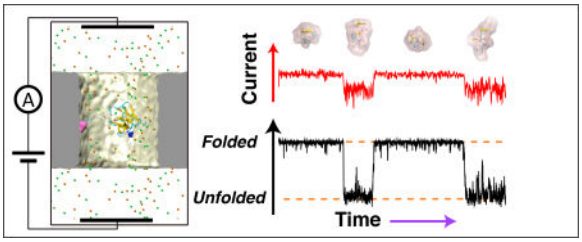

Keywords

Nanopore; protein folding; ionic current; molecular dynamics; folding intermediates; misfolding

[*]To whom correspondence should be addressed: aksiment@illinois.edu.

Supporting Information Available

Detailed description of additional systems used for MD simulations of ionic current blockade, physical properties of proteins considered in this work, calculation of ion concentration and mobility distributions, fraction of the nanopore volume occupied by the protein, theoretical model of ionic current blockades, calculations of rotation-averaged ionic currents, theory *versus* simulation at variable electrolyte conditions, the effect of temperature on the ionic current difference, real-time detection of folding-unfolding transitions, the effect of protein conformation, trajectory-averaged blockade currents, characterization of protein folding intermediates. This material is available free of charge *via* the internet at http://pubs.acs.org.

Folding of a peptide chain into a three-dimensional structure is one of the most fundamental biological processes.[1] Disruption of the folding process, through either a chance mutation or interfering interaction with other components of the cell, have been implicated in a number of heath disorders,[2] most notably in Parkinson's[2,3] and Alzheimer's[4] deseases. Conversely, controlling or disrupting protein folding pathways by designer molecules offers a means for development of therapeuticals.[5] With respect to the latter, knowing the protein folding pathway, the molecular structure of the folding intermediates and their susceptibility to a drug's interfering interaction is paramount.

Experimental studies of protein folding have a long and rich history.[1,6–10] Differential scanning calorimetry characterizes energetics of protein folding by measuring the excess heat produced by the folding process.[11] A flash of a laser beam[12] or a rapid change of pressure[13] can trigger a protein folding or unfolding transition, which, in combination with an optical measurement, can report on the folding/unfolding rates[14] or allow the folding kinetics to be monitored in real time.[10] Protein folding dynamics can be probed by the nuclear magnetic resonance method,[15] which associates broadening or shifting of site-specific resonances with protein folding states. These ensemble measurements, however, monitor folding/unfolding of many proteins in parallel, which obscures folding intermediates as they form spontaneously and asynchronously throughout the sample.

Single-molecule methods, such as atomic force microscopy,[16] optical tweezers[17] and fluorescence resonance energy transfer[8,18] measurements can characterize folding or unfolding of individual proteins, providing both equilibrium and kinetic information. However, the small energy difference of the folding intermediates and the short (microseconds to milliseconds) timescale of conformation transitions complicates characterization of the protein folding intermediates.[19] Furthermore, such single-molecule measurements require elaborate labeling and presently lack throughput. Various computational methods[6,20–22] and, recently, brute-force all-atom MD simulations,[23,24] have been successful in predicting the folding state of a protein and characterizing the folding intermediates. However, fully atomistic simulations remain computationally expensive and their application is presently limited to rather small proteins.

The nanopore sensing principle[25,26] offers both high-throughput and label-free characterization of single molecules.[27] In a typical nanopore measurement, biomolecules are driven through a nanopore one at a time by an external electric field, modulating the nanopore ionic current that reports on the presence and identity of the biomolecules. The sub-Ångstrom precision of a nanopore measurement[28] and its sub-microsecond temporal resolution[29] makes a nanopore measurement an attractive tool for the characterization of proteins. Indeed, nanopores have been successfully used to detect and characterize single proteins,[30–37] including individual amino acids[38,39] and proteins bound to DNA.[40–44]

Several groups have reported nanopore measurements of protein unfolding produced by denaturing agents,[32,45–48] temperature,[49,50] pH,[51] transmembrane bias[52] or even molecular motors.[53,54] There is, however, no consensus on the effect of protein unfolding on the ionic current level. For example, several groups found proteins to block the nanopore ionic current

more in their unfolded state than in the folded one,[46,54,55] however, the opposite was also reported,[32,47] which could be partially explained by the differences in the pore geometry[46,47,54] and applied bias conditions.[32,52] In general, interpretation of ionic current blockades produced by the translocation of untethered proteins is complicated by the bandwidth limitation of a nanopore measurement,[35] interaction of the proteins with the nanopore surface[56] and the unknown orientation of the protein during the translocation. At a fundamental level, the physical mechanism that could give rise to an ionic current signal indicative of a protein's folding/unfolding transition was not known.

Here, we report results of all-atom molecular dynamics (MD) simulations that directly evaluated the effect of protein folding on the nanopore ionic current. Analysis of the MD trajectories elucidated the magnitude of the effect, its dependence on the molecular weight of the protein, buffer conditions and temperature. Using a theoretical model, we show that the effect is caused by the reduction of ion mobility in proximity to a protein surface, and that the effect remains detectable despite orientational and conformational heterogeneity of the folded and unfolded states. Finally, we use all-atom MD trajectories of protein folding to demonstrate the feasibility of real-time, single-molecule detection of protein folding.

RESULTS AND DISCUSSION

MD simulations of ionic current through a nanopore blocked by a protein directly demonstrate the possibility of distinguishing the protein folding state *via* ionic current measurement. In a typical simulation system, Figure 1A, a protein, in either its folded or unfolded conformation, was held at the center of a solid-state nanochannel containing electrolyte solution. An electric field (300 mV/~4 nm) was applied along the symmetry axis of the nanochannel, producing the ionic current. To reduce the statistical uncertainty of the ionic current determination, the protein atoms were constrained to their initial coordinates, which suppressed conformational fluctuations, see Methods for details. The ionic currents recorded from a 150 ns simulations of the folded, I_f, and unfolded, I_{unf}, states of the protein, Figure 1B, were considerably lower than the current recorded in the absence of the protein (the open pore current, I_0). Most importantly, the blockade current generated by the folded protein was significantly higher than the current recorded for the unfolded protein. Hereafter, we will refer to the ionic current difference produced by the folding state of the protein as $\Delta I_F = I_f - I_{unf}$. Repeating the simulations for eight additional proteins produced similar outcome Figure 1C: the blockade current in the folded state, I_f, was higher than the blockade current in the unfolded state, I_{unf}, or $\Delta I_F > 0$. Repeating simulations for three different orientations of the titin protein in both folded and unfolded states, Supporting Information (SI) Figure S1B, and for four additional conformations of the unfolded HP35 protein, SI Figure S1C, provided further support to the above conclusion. SI Tables S1 and S2 provide detailed information about all proteins considered in this work.

Further simulations and analyses elucidated the microscopic origin of the blockade current dependence on the folding state of a protein. First, we note that the physical volume occupied by a protein does not change with its folding state in our simulations, as the systems containing the folded and unfolded structures have identical numbers of water molecules and ions. To elucidate the effect of a protein surface on ionic conductivity of

nearby electrolyte solution, we performed additional simulations of three proteins (titin, BBL and λ-repressor) submerged in a bulk electrolyte and subject to an electric field; SI Figure S2A illustrates typical simulation systems. As in the case of the nanochannel simulations, proteins were restrained to maintain their initial conformations. The resulting MD trajectories were analyzed to determine the dependence of the local ion concentration C and ion mobility μ on the distance from the protein surface, r, Figure 2A.

Similar to the dependence previously reported for DNA,[57,58] the ion concentration and mobility sharply decrease near a protein surface, Figure 2B and SI Figure S2B; SI Methods 1 describes the analysis methods. Remarkably, both $C(r)$ and $\mu(r)$ dependences do not depend, within the statistical error, on the folding state of the protein nor on the ion type; the lack of ion type dependence can be attributed to the weak charge density of the proteins, SI Table S1. The plots also reveal that both C and μ reach bulk electrolyte values at distance r^*=6.6 Å. As the electrolyte conductivity, σ, is proportional to both C and μ, the sharp reduction of C and μ near the protein surface can explain the ionic current difference produced by protein folding if the volume affected by the C and μ reductions is larger for the unfolded state than for the folded one. Figure 2C plots the fractions of the nanopore volume occupied by the protein and the solvent molecules surrounding the protein within distance r of the protein surface for both folded and unfolded states of the protein. For r = 0, the volume fractions are the same, however, as r values approach r^*, the volume occupied by the unfolded protein and the surrounding solvent increases faster than the volume occupied by the folded protein, which is consistent with the more expanded conformation of the former. Similar dependences are observed for eight other proteins, SI Figure S3.

To quantitatively prove that the ionic current difference produced by protein folding originates from the reduction in ion mobility and concentration near the protein surface, we developed a theoretical model that could predict the ionic current of a weakly charged protein from its atomic coordinates, Figure 3. The ionic current $I = V/R$, where V is the transmembrane bias and R is the resistance of the nanopore containing a protein. To compute the nanopore resistance, the nanopore volume was divided into cylindrical segments concentric with the nanopore axis; each of the segments was further divided into a collection of 1 Å^3 cubes, Figure 3A. The resistance of cube j in cylindrical segment i, $R_{ij} = l_{ij}/(\sigma(r_{ij})S_{ij})$, where l_{ij} and S_{ij} are the length and the cross sectional area of the cube, respectively, and $\sigma(r_{ij})$ is the local conductivity of the cube assumed to be a function of distance to the nearest protein surface, r_{ij}. The local conductivity derived from the analysis of the MD trajectories, Figure 3A (right), is in agreement with this assumption. The resistance of one nanopore segment R_i is then $1/R_i = \sum_{j=1}^{m} 1/R_{ij}$, where m is the number of cubes in segment i. The resistance of the entire nanopore is $R = \sum_{j=1}^{n} R_i$, where n is the number of cylindrical segments. Note that our model does not take into account the effects of access resistance[59] and nanopore charge,[60] which is justified by the properties of the all-atom models considered in this work. A similar model was previously used to predict ionic current blockades produced by DNA in a double nanopore system.[61]

Knowing the atomic coordinates of a protein and how the local ion conductivity depends on the distance from the protein surface, we used the model to compute the blockade current for

the nine proteins in their folded and unfolded states, Figure 3B. SI Methods 2 provides a detailed description of the numerical procedures. The currents predicted by the model are in excellent agreement with the currents measured from brute-force MD simulations for both folded and unfolded states of the protein, Figure 3B. Furthermore, our theoretical model predicts the blockade current differences ΔI_F rather well, Figure 3C, taking into account the statistical accuracy of the ionic current determination by the brute-force MD method. Similar agreement between the two methods was observed for ionic currents recorded from the simulations of bulk electrolyte systems, SI Figure S4. The good agreement between theory and simulation indicates that the ionic current difference produced by the folding state of a protein is indeed determined by the reduction in ion mobility and concentration near the protein surface, which is larger in the case of an unfolded protein.

It was previously suggested that the orientation of a protein inside a nanopore could affect the ionic current blockade.[56,62] To determine the effect of protein orientation on the blockade current difference produced by the folding state of a protein, we applied our theoretical model to compute the blockade currents for 1728 unique orientations of a protein in both folded and unfolded states, Figure 4A; see SI Methods 3 for a detailed description of the calculations. Indeed, the protein's orientation is seen to affect the blockade current considerably, Figure 4B, with the unfolded state current affected more. Despite the dependence of the ionic current on protein orientation, the ionic current blockades produced by the folded and unfolded states could be easily distinguished. Clear separation of the rotation-averaged currents was observed for seven other proteins; considerable overlap of the rotation-averaged I_f and I_{unf} values was seen for the α3D protein, SI Figure S6, which is the most asymmetric protein considered in this work (see SI table S1). Figure 4C plots the rotation-averaged current blockade amplitudes $I_0 - I_f$ and $I_0 - I_{unf}$ for the nine proteins considered as a function of molecular weight. As expected, the current blockade amplitudes increase with the molecular weight of the protein for both folded and unfolded states. The blockade current difference ΔI_F, however, does not show a strong dependence on the molecular weight, Figure 4D, likely because of the insufficient conformational sampling of the unfolded state.[63]

So far, all our ionic current simulations were carried out at a high electrolyte concentration (2 M KCl) which provides the best condition for the discrimination of ionic current levels. However, not all proteins are stable in high ionic strength electrolytes. To determine the effect of electrolyte concentration of the ionic current difference ΔI_F, we repeated our all-atom MD simulations of the ionic current through the nanochannel containing either Trp-cage or λ-repressor proteins at 0.1, 0.3 and 1 M KCl conditions. The ionic current dependence between the folded and unfolded states of the proteins, ΔI_F, is seen to increase with electrolyte concentration, Figure 4E (inset); similar ΔI_F values were obtained for both proteins despite their different molecular weights, which we attribute to using a fixed (random) orientation of the proteins in the all-atom simulations. To obtain rotation-averaged data, Figure 4E, we applied our theoretical model to the two proteins, taking into account the electrolyte conditions by adjusting the bulk conductivity value, σ_0, without modifying the functional dependence of $\sigma(r)/\sigma_0$ on the distance from the protein surface (see Figure 3A). The ionic current predicted by the modified model matched the all-atom MD data remarkably well without any further adjustments, SI Figure S8. In agreement with our 2 M

KCl data, Figure 4D, the larger protein (λ-repressor) is found to produce a larger blockade current difference, indicative of protein folding regardless of the ionic conditions, Figure 4E. The dependence of ΔI_F on ion concentration is non-linear, but follows the non-liner dependence of ion conductivity on ion concentration.

Temperature is commonly used to control folding-unfolding transitions.[12] To determine the effect of temperature on ΔI_F, we repeated all-atom MD simulations of the nanochannel system containing the Trp-cage protein at 283, 313, 333 and 363 K and 2 M KCl. The blockade currents I_f and I_{unf} are both found to increase with the temperature,[64] SI Figure S9A, with the difference of the currents, ΔI_F, increasing as well, Figure 4F. Scaled with the open pore current, the relative current blockade ($\Delta I/I_0$, SI Figure S9B) and the relative current difference ($\Delta I_F/I_0$, Figure 4F) decrease with the temperature, similar to the dependence observed in DNA translocation experiment.[65] We attribute reduction of the scaled blockade current difference with increasing temperature to the temperature dependence on ion mobility.[66] With small modifications, our theoretical model is able to describe ionic current blockades at arbitrary temperature, SI Figure S9C–D.

To directly demonstrate the feasibility of real-time detection and characterization of protein folding-unfolding transitions, we used millisecond all-atom MD trajectories of protein folding-unfolding transitions[24,67] to predict ionic current signals that would have been recorded if those folding-unfolding transitions were to happen inside a nanopore. In doing so, we relied on the separation of time scales associated with ion transport and conformational fluctuation[68] which permitted us to use our theoretical model to compute a set of "exact" ionic current values for an ensemble of static conformations realized during the protein folding simulations, see SI Methods 4 for technical details. We have also neglected a possibility of nanopore confinement affecting the protein folding pathway.[69] Figures 5A–C show the ionic current traces produced by Trp-cage, NTL9 and ubiquitin proteins placed inside the nanopore (top) along with the folding parameter Q (bottom), which reports on the fraction of native contacts in a given protein conformation: $Q = 0$ or $Q = 1$ indicates a completely unfolded or folded conformation, respectively (see SI Methods 4 for a mathematical formulation). Additional traces for the Trp-cage, NTL9 and ubiquitin systems as well as the data for BBL, protein G, α3D and λ-repressor are shown in SI Figures S10–S15. In all cases, the blockade current exhibits rapid transitions between two levels correlated with the transitions in the folding parameter, which unambiguously associate the two ionic current levels with the protein being in either a folded or unfolded state. Similar anti-correlations are observed when comparing the blockade current to either the protein radius of gyration or the root-mean-square deviation (RMSD) from the folded state, SI Figure S16. Consistent with our previous observation, proteins are found to block the current the least in their completely folded state. Note that no orientational or conformational selection or transformation was used to compute the ionic current traces and, hence, the fluctuations of the ionic current in either folded or unfolded states reflect the conformational degrees of freedom of the proteins, which could be used to independently evaluate rotation/conformation-averaged values of the blockade currents (see SI Figures S7D–F, S17 and S18).

Statistical analysis of the ionic current recordings suggests the possibility of the detection and characterization of protein folding intermediates. In Figures 5D–F, we plot the difference between the current blockade of a protein folding intermediate and the current blockade of a fully folded state, $I - I_f$, averaged over all folding intermediates having the prescribed values of the protein folding parameter Q, the protein's radius of gyration, R_g, and the RMSD of the protein's coordinates from the folded state, for Trp-cage, NTL9 and ubiquitin. Starting from a negative value ($I_{unf} < I_f$), the ionic current difference increases monotonically as the protein folding progresses, Figure 5D. The current blockades become deeper as the protein unfolds, Figure 5E, however, the dependence of $I - I_f$ on R_g is clearly non-linear, with more pronounced changes in the ionic current occurring closer to the folded states. The ionic current difference decreases linearly with RMSD from the folded state, Figure 5F. Very similar dependences are observed from the statistical analysis of the millisecond folding trajectories of four other proteins (BBL, protein G, α3D and λ-repressor, SI Figure S19) and from the analysis of replica-exchange simulations of villin head piece (HP35) and WW domain (GTT) folding,[63] SI Figure S20. Thus, knowing the ionic current levels for the folded and unfolded state of a protein, intermediate states of the protein folding process can be characterized *via* nanopore ionic current measurement.

CONCLUSIONS

In this study, we have theoretically shown that measurements of nanopore ionic current can be used to monitor, in real time, folding-unfolding transitions of a protein and to characterize intermediate states along a protein folding pathway. The experimental detection of protein folding can be realized by collecting ionic current signatures of many proteins transiently passing, one-by-one, through the nanopore volume.[32,46] While offering high throughput, this approach, however, relies on statistical averaging over many protein translocation events, which eliminates some of the advantages of a single-molecule measurement. A much more attractive possibility is continuous monitoring of the ionic current through a nanopore that has a protein attached to its surface.[33,70] Lipid-coated nanopore systems[33,62] are particularly suitable for such measurements, as they can retain proteins within the nanopore volume long enough to detect a folding-unfolding transition in real time while allowing different copies of the proteins to enter and leave the nanopore. Decorated with metallic nanoantennas, plasmonic nanopores[71] can be used to both rapidly change the temperature of a nanopore volume[65,72,73] and to trap proteins,[74] offering a single-molecule realization of a temperature jump experiment. By performing such ionic current measurements using nanopores of different sizes, one may be able to elucidate the effect of confinement on the protein folding process.[2] All of the above suggest that real time monitoring of protein folding-unfolding transition using an experimental nanopore system can be realized in the nearest future, leading to exciting developments in the area of molecular diagnostics and drug design.

METHODS

General MD Methods

All simulations were performed using the classical MD package NAMD,[75] periodic boundary conditions and a 2 fs timestep. The CHARMM36 force field[76] with non-bonded

corrections for ions[77] were used to describe carbon atoms (type CA), proteins, TIP3P water and ions. RATTLE[78] and SETTLE[79] algorithms were applied to covalent bonds that involved hydrogen atoms in protein and water molecules, respectively. The particle-Mesh-Ewald (PME)[80] algorithm was adopted to evaluate the long-range electrostatic interaction over a 1 Å-spaced grid. Van der Waals interactions were evaluated using a smooth 10–12 Å cutoff. Langevin dynamics were used to maintain the temperature at 293 K (or other temperatures if specified). Multiple time stepping was used to calculate local interactions every time step and full electrostatics every three time steps.

MD Simulations of Nanopore Systems—The twelve-layer hexagonal graphene membrane was generated using the Inorganic Builder plugin in VMD.[81] The nanopore was created by removing atoms that satisfy the condition $x^2 + y^2 < (d/2)^2$, where x and y were the coordinates of the graphene atoms and $d = 6$ nm was the target diameter of the nanopore. Proteins (one per system) were placed in the nanochannel with their centers of mass located at the nanopore axis. The atomic structures of folded proteins Trp-cage, HP35, GTT, NTL9, BBL, protein G, α3D, ubiquitin, λ-repressor and BBA were taken from the Protein Data Bank, entries 2JOF, 2F4K, 2F21, 2HBA, 2WXC, 1MIO, 2A3D, 1UBQ, and 1LMB, 1FME, respectively.[24,63,67] Mutants of folded Trp-cage, NTL9, protein G and λ-repressor were generated to match the proteins used by the D.E. Shaw group.[24] The unfolded structures of Trp-cage, NTL9, BBL, protein G, α3D, ubiquitin, λ-repressor and BBA were taken from the MD trajectories generated by the D.E. Shaw group;[24,67] the unfolded structures of HP35 and GTT were taken from the REMD trajectories generated by Jejoong Yoo;[63] all unfolded conformations had Q value less than 0.1. The systems were solvated by VMD's Solvate plugin; water molecules overlapping with the membrane and the protein were removed. Potassium and chloride ions were added to neutralize the system and bring the ion concentration to 2 M. Each final system contained ~ 19,000 atoms. Following assembly, each system was minimized for 9,600 steps using the conjugate gradient method and equilibrated for 12 ns in the constant number of atoms, volume and temperature (NVT) ensemble. For each system containing a folded protein, a set of simulations was performed varying the number of water molecules within the channel to reproduce the water density observed in bulk simulations at atmospheric pressure. The unfolded protein systems contained the same number of water molecules as the respective folded protein systems. Langevin thermostat was applied to the atoms of the graphene membrane with a damping coefficient of 1.0 ps^{-1}. In all simulations, atoms of the membrane were harmonically restrained to their initial coordinates; the spring constant of each restraint was 20 kcal mol^{-1} Å $^{-2}$. Coordinates of the protein atoms were fixed to their initial values. Following equilibrations, the systems were simulated in the NVT ensemble for ~ 150 ns under a 300 mV bias voltage applied across the ~4-nm thick carbon membrane. The same protocols were followed to set up open pore systems (containing no protein), systems at different temperatures (283 K, 313 K, 333 K and 363 K) and electrolyte conditions (0.1 M, 0.3 M and 1.0 M KCl).

MD Simulations of Proteins in Bulk Electrolytes—In addition to nanopore simulations, several proteins (titin, BBL and λ-repressor) were simulated in bulk electrolytes. The systems were prepared by solvating and ionizing atomic-scale models of

the proteins in their folded or unfolded states. The folded and unfolded structures of BBL and λ-repressor are the same as those used in nanopore systems. The folded structure of titin was taken from PDB entry 1TIT and the unfolded structure of titin was taken from MD trajectories from Shalini John Lovis in our group (the paper has been submitted for review). Each system was a cube ~9.7 nm on each side and contained ~ 92,000 atoms. The systems underwent 9600 steps of minimization and subsequent 12 ns equilibration in the constant number of particles, pressure and temperature (NPT) ensemble. Nose-Hoover Langevin piston pressure control[82] was used to maintain the pressure at 1 atm; temperature was maintained by the Langevin thermostat applied to all non-hydrogen atoms of the system. The simulations under applied an electric field (500 mV bias over the unit cell length) were performed in the NVT ensemble for 30 ns.

Ionic Current Calculation—Coordinates of all atoms in the systems were recorded every 2.4 picoseconds. The ionic current was calculated as:[66]

$$I(t)=\frac{1}{\delta \mathrm{t} \mathrm{L}_z}\sum_{j=1}^{N} q_{\mathrm{j}}\delta z_{\mathrm{j}}(t) \quad (1)$$

where

$$\delta z_{\mathrm{j}}(t)=\begin{cases} z_{\mathrm{j}}(t+\delta t)-z_{\mathrm{j}}(t), |z_{\mathrm{j}}(t+\delta t)-z_{\mathrm{j}}(t)|<L_{\mathrm{z}}/2 \\ z_{\mathrm{j}}(t+\delta t)-z_{\mathrm{j}}(t)+L_{\mathrm{z}}, z_{\mathrm{j}}(t+\delta t)-z_{\mathrm{j}}(t)<-L_{\mathrm{z}}/2 \\ z_{\mathrm{j}}(t+\delta t)-z_{\mathrm{j}}(t)-L_{\mathrm{z}}, z_{\mathrm{j}}(t+\delta t)-z_{\mathrm{j}}(t)>L_{\mathrm{z}}/2 \end{cases} \quad (2)$$

is the displacement of ion j along the z direction during the time interval δt; z_{j} and q_{j} are the z coordinate and the charge of ion j, respectively; δt=2.4 ps; L_z is the length of the graphene nanopore in the z direction; and the sum runs over all ions.

Supplementary Material

Refer to Web version on PubMed Central for supplementary material.

Acknowledgments

This work was supported by a grant from the National Institutes of Health (R01-HG007406). The authors acknowledge supercomputer time at the Blue Waters Sustained Petascale Facility (University of Illinois) and at the Texas Advanced Computing Center (Stampede, allocation award MCA05S028). W.S. acknowledges financial support from the China Scholarship Council (CSC201506090040) and the National Natural Science Foundation of China (Grant No.51435003). The authors thank the D.E. Shaw group for sharing the all-atom trajectories of protein folding and Jejoong Yoo for assistance with analysis of replica-exchange simulations.

References

1. Dill KA, MacCallum JL. The Protein-Folding Problem, 50 Years On. Science. 2012; 338:1042. [PubMed: 23180855]
2. Hartl F, Bracher A, Hayer-Hartl M. Molecular Chaperones in Protein Folding and Proteostasis. Nature. 2011; 475:324–332. [PubMed: 21776078]

3. Selkoe DJ. Cell Biology of Protein Misfolding: The Examples of Alzheimer's and Parkinson's Diseases. Nat. Cell. Biol. 2004; 6:1054–1061. [PubMed: 15516999]
4. Nasica-Labouze J, Nguyen PH, Sterpone F, Berthoumieu O, Buchete N-V, Cote S, De Simone A, Doig AJ, Faller P, Garcia A, et al. Amyloid β Protein and Alzheimer's Disease: When Computer Simulations Complement Experimental Studies. Chem. Rev. 2015; 115:3518–3563. [PubMed: 25789869]
5. Balch WE, Morimoto RI, Dillin A, Kelly JW. Adapting Proteostasis for Disease Intervention. Science. 2008; 319:916–919. [PubMed: 18276881]
6. Fersht AR, Daggett V. Protein Folding and Unfolding at Atomic Resolution. Cell. 2002; 108:573–582. [PubMed: 11909527]
7. Dobson CM. Protein Folding and Misfolding. Nature. 2003; 426:884–90. [PubMed: 14685248]
8. Royer CA. Probing Protein Folding and Conformational Transitions with Fluorescence. Chem. Rev. 2006; 106:1769–1784. [PubMed: 16683754]
9. Walter P, Ron D. The Unfolded Protein Response: From Stress Pathway to Homeostatic Regulation. Science. 2011; 334:1081–1086. [PubMed: 22116877]
10. Englander SW, Mayne L. The Nature of Protein Folding Pathways. Proc. Natl. Acad. Sci. U. S. A. 2014; 111:15873–15880. [PubMed: 25326421]
11. Johnson CM. Differential Scanning Calorimetry as a Tool for Protein Folding and Stability. Arch. Biochem. Biophys. 2013; 531:100–109. [PubMed: 23022410]
12. Gruebele M, Sabelko J, Ballew R, Ervin J. Laser Temperature-Jump Induced Protein Refolding. Accts. Chem. Res. 1998; 31:699–707.
13. Dumont C, Emilsson T, Gruebele M. Reaching the Protein Folding Speed Limit with Large, Sub-Microsecond Pressure Jumps. Nat. Methods. 2009; 6:515–519. [PubMed: 19483692]
14. Mayor U, Johnson V, Daggett CM, Fersht AR. Protein Folding and Unfolding in Microseconds to Nanoseconds by Experiment and Simulation. Proc. Natl. Acad. Sci. U. S. A. 2000; 97:13518–13522. [PubMed: 11087839]
15. Dyson HJ, Wright PE. Unfolded Proteins and Protein Folding Studied by NMR. Chem. Rev. 2004; 104:3607–3622. [PubMed: 15303830]
16. Rief M, Gautel M, Oesterhelt F, Fernandez JM, Gaub HE. Reversible Unfolding of Individual Titin Immunoglobulin Domains by AFM. Science. 1997; 276:1109–1112. [PubMed: 9148804]
17. Tskhovrebova L, Trinick J, Sleep JA, Simmons RM. Elasticity and Unfolding of Single Molecules of the Giant Protein Titin. Nature. 1997; 387:308–312. [PubMed: 9153398]
18. Weiss S. Fluorescence Spectroscopy of Single Biomolecules. Science. 1999; 283:1676–1683. [PubMed: 10073925]
19. Meinhold DW, Wright PE. Measurement of Protein Unfolding/Refolding Kinetics and Structural Characterization of Hidden Intermediates by NMR Relaxation Dispersion. Proc. Natl. Acad. Sci. U. S. A. 2011; 108:9078–9083. [PubMed: 21562212]
20. Dill KA, Bromberg S, Yue K, Chan HS, Ftebig KM, Yee DP, Thomas PD. Principles of Protein Folding - a Perspective from Simple Exact Models. Protein Sci. 1995; 4:561–602. [PubMed: 7613459]
21. Onuchic JN, Luthey-Schulten Z, Wolynes PG. Theory of Protein Folding: The Energy Landscape Perspective. Annu. Rev. Phys. Chem. 1997; 48:545–600. [PubMed: 9348663]
22. Pande VS, Baker I, Chapman J, Elmer SP, Khaliq S, Larson SM, Rhee YM, Shirts MR, Snow CD, Sorin EJ, Zagrovic B. Atomistic Protein Folding Simulations on the Submillisecond Time Scale Using Worldwide Distributed Computing. Biopolymers. 2003; 68:91–109. [PubMed: 12579582]
23. Shaw DE, Maragakis P, Lindorff-Larsen K, Piana S, Dror RO, Eastwood MP, Bank JA, Jumper JM, Salmon JK, Shan Y, Wriggers W. Atomic-Level Characterization of the Structural Dynamics of Proteins. Science. 2010; 330:341–346. [PubMed: 20947758]
24. Lindorff-Larsen K, Piana S, Dror RO, Shaw DE. How Fast-Folding Proteins Fold. Science. 2011; 334:517–520. [PubMed: 22034434]
25. Bezrukov SM, Vodyanoy I, Parsegian VA. Counting Polymers Moving through a Single Ion Channel. Nature. 1994; 370:279–281. [PubMed: 7518571]

26. Kasianowicz JJ, Brandin E, Branton D, Deamer DW. Characterization of Individual Polynucleotide Molecules Using a Membrane Channel. Proc. Natl. Acad. Sci. U. S. A. 1996; 93:13770–13773. [PubMed: 8943010]
27. Howorka S, Siwy ZS. Nanopore Analytics: Sensing of Single Molecules. Chem. Soc. Rev. 2009; 38:2360–2384. [PubMed: 19623355]
28. Derrington IM, Craig JM, Stava E, Laszlo AH, Ross BC, Brinkerhoff H, Nova IC, Doering K, Tickman BI, Ronaghi M, Mandell JG, Gunderson KL, Gundlach JH. Subangstrom Single-Molecule Measurements of Motor Proteins Using a Nanopore. Nat. Biotech. 2015; 33:1073–1075.
29. Shekar S, Niedzwiecki DJ, Chien C-C, Ong P, Fleischer DA, Lin JK, Rosenstein J, Drndic M, Shepard KL. Measurement of DNA Translocation Dynamics in a Solid-State Nanopore at 100 ns Temporal Resolution. Nano Lett. 2016; 16:4483–4489. [PubMed: 27332998]
30. Movileanu L, Howorka S, Braha O, Bayley H. Detecting Protein Analytes that Modulate Transmembrane Movement of a Polymer Chain Within a Single Protein Pore. Nat. Biotech. 2000; 18:1091–1095.
31. Mohammad M, Prakash S, Matouschek A, Movileanu L. Controlling a Single Protein in a Nanopore through Electrostatic Traps. J. Am. Chem. Soc. 2008; 130:4081–4088. [PubMed: 18321107]
32. Talaga DS, Li J. Single-Molecule Protein Unfolding in Solid-State Nanopores. J. Am. Chem. Soc. 2009; 131:9287–9297. [PubMed: 19530678]
33. Yusko EC, Johnson JM, Majd S, Prangkio P, Rollings RC, Li J, Yang J, Mayer M. Controlling Protein Translocation through Nanopores with Bio-inspired Fluid Walls. Nat. Nanotech. 2011; 6:253–260.
34. Freedman KJ, Bastian AR, Chaiken I, Kim MJ. Solid-State Nanopore Detection of Protein Complexes: Applications in Healthcare and Protein Kinetics. Small. 2012; 9:750–759. [PubMed: 23074081]
35. Plesa C, Kowalczyk SW, Zinsmeester R, Grosberg AY, Rabin Y, Dekker C. Fast Translocation of Proteins through Solid State Nanopores. Nano Lett. 2013; 13:658–663. [PubMed: 23343345]
36. Larkin J, Henley RY, Muthukumar M, Rosenstein JK, Wanunu M. High-Bandwidth Protein Analysis Using Solid-State Nanopores. Biophys. J. 2014; 106:696–704. [PubMed: 24507610]
37. Biesemans A, Soskine M, Maglia G. A Protein Rotaxane Controls the Translocation of Proteins Across a ClyA Nanopore. Nano Lett. 2015; 15:6076–6081. [PubMed: 26243210]
38. Zhao Y, Ashcroft B, Zhang P, Liu H, Sen S, Song W, Im J, Gyarfas B, Manna S, Biswas S, Borges C, Lindsay S. Single-Molecule Spectroscopy of Amino Acids and Peptides by Recognition Tunnelling. Nat. Nanotech. 2014; 9:466–473.
39. Rosen CB, Rodriguez-Larrea D, Bayley H. Single-Molecule Site-Specific Detection of Protein Phosphorylation with a Nanopore. Nat. Biotech. 2014; 32:179–181.
40. Hornblower B, Coombs A, Whitaker RD, Kolomeisky A, Picone SJ, Meller A, Akeson M. Single-Molecule Analysis of DNA-Protein Complexes Using Nanopores. Nat. Mater. 2007; 4:315–317.
41. Zhao Q, Sigalov G, Dimitrov V, Dorvel B, Mirsaidov U, Sligar S, Aksimentiev A, Timp G. Detecting SNPs Using a Synthetic Nanopore. Nano Lett. 2007; 7:1680–1685. [PubMed: 17500578]
42. Kowalczyk SW, Hall AR, Dekker C. Detection of Local Protein Structures along DNA Using Solid-State Nanopores. Nano Lett. 2010; 10:324–328. [PubMed: 19902919]
43. Plesa C, Ruitenberg JW, Witteveen MJ, Dekker C. Detection of Individual Proteins Bound along DNA Using Solid-State Nanopores. Nano Lett. 2015; 15:3153–3158. [PubMed: 25928590]
44. Kong J, Bell NAW, Keyser UF. Quantifying Nanomolar Protein Concentrations Using Designed DNA Carriers and Solid-state Nanopores. Nano Lett. 2016; 16:3557–3562. [PubMed: 27121643]
45. Oukhaled AO, Mathé J, Biance A-L, Bacri L, Betton J-M, Lairez D, Pelta J, Auvray L. Unfolding of Proteins and Long Transient Conformations Detected by Single Nanopore Recording. Phys. Rev. Lett. 2007; 98:158101. [PubMed: 17501386]
46. Freedman KJ, Jurgens M, Prabhu A, Ahn CW, Jemth P, Edel JB, Kim MJ. Chemical, Thermal, and Electric Field Induced Unfolding of Single Protein Molecules Studied Using Nanopores. Anal. Chem. 2011; 83:5137–5144. [PubMed: 21598904]

47. Li J, Fologea D, Rolling R, Ledden B. Characterization of Protein Unfolding with Solid-State Nanopores. Prot. Pept. Lett. 2014; 21:256–265.
48. Pastoriza-Gallego M, Breton M-F, Discala F, Auvray L, Betton J-M, Pelta J. Evidence of Unfolded Protein Translocation through a Protein Nanopore. ACS Nano. 2014; 8:11350–11360. [PubMed: 25380310]
49. Payet L, Martinho M, Pastoriza-Gallego M, Betton J-M, Auvray L, Pelta J, Mathe J. Thermal Unfolding of Proteins Probed at the Single Molecule Level Using Nanopores. Anal. Chem. 2012; 84:4071–4076. [PubMed: 22486207]
50. Abdelghani O, Manuela P-G, Laurent B, Jerome M, Loic A, Juan P. Protein Unfolding Through Nanopores. Prot. Pept. Lett. 2014; 21:266–274.
51. Mereuta L, Roy M, Asandei A, Lee JK, Park Y, Andricioaei I. Slowing Down Single-Molecule Trafficking through a Protein Nanopore Reveals Intermediates for Peptide Translocation. Sci. Reports. 2014; 4:3885.
52. Freedman KJ, Haq SR, Edel JB, Jemth P, Kim MJ. Single Molecule Unfolding and Stretching of Protein Domains inside a Solid-State Nanopore by Electric Field. Sci. Reports. 2013; 3:1638.
53. Nivala J, Marks DB, Akeson M. Unfoldase-Mediated Protein Translocation through an α-Hemolysin Nanopore. Nat. Biotech. 2013; 31:247–250.
54. Rodriguez-Larrea D, Bayley H. Multistep Protein Unfolding During Nanopore Translocation. Nat. Nanotech. 2013; 8:288–295.
55. Jung Y, Bayley H, Movileanu L. Temperature-Responsive Protein Pores. J. Am. Chem. Soc. 2006; 128:15332–15340. [PubMed: 17117886]
56. Niedzwiecki DJ, Grazul J, Movileanu L. Single-Molecule Observation of Protein Adsorption onto an Inorganic Surface. J. Am. Chem. Soc. 2010; 132:10816–10822. [PubMed: 20681715]
57. Comer J, Aksimentiev A. Predicting the DNA Sequence Dependence of Nanopore Ion Current Using Atomic-Resolution Brownian Dynamics. J. Phys. Chem. C. 2012; 116:3376–3393.
58. Kesselheim S, Müller W, Holm C. Origin of Current Blockades in Nanopore Translocation Experiments. Phys. Rev. Lett. 2014; 112:018101. [PubMed: 24483933]
59. Kowalczyk SW, Grosberg AY, Rabin Y, Dekker C. Modeling the Conductance and DNA Blockade of Solid-State Nanopores. Nanotech. 2011; 22:315101.
60. Smeets RMM, Keyser UF, Krapf D, Wu M-Y, Dekker NH, Dekker C. Salt-Dependence of Ion Transport and DNA Translocation through Solid-state Nanopores. Nano Lett. 2006; 6:89–95. [PubMed: 16402793]
61. Pud S, Chao S-H, Belkin M, Verschueren D, Huijben T, van Engelenburg C, Dekker C, Aksimentiev A. Mechanical Trapping of DNA in a Double-Nanopore System. Nano Lett. 2016; 16:8021–8028. [PubMed: 27960493]
62. Yusko EC, Bruhn BR, Eggenberger OM, Houghtaling J, Rollings RC, Walsh NC, Nandivada S, Pindrus M, Hall AR, Sept D, Li J, Kalonia DS, Mayer M. Real-Time Shape Approximation and Fingerprinting of Single Proteins Using a Nanopore. Nat. Nanotech. 2017; 12:360–367.
63. Yoo J, Aksimentiev A. Refined Parameterization of Nonbonded Interactions Improves Conformational Sampling and Kinetics of Protein Folding Simulations. J. Phys. Chem. Lett. 2016; 7:3812–3818. [PubMed: 27617340]
64. Chimerel C, Movileanu L, Pezeshki S, Winterhalter M, Kleinekathofer U. Transport at the Nanoscale: Temperature Dependence of Ion Conductance. Eur. Biophys. J. 2008; 38:121–125. [PubMed: 18726094]
65. Nicoli F, Verschueren D, Klein M, Dekker C, Jonsson MP. DNA Translocations through Solid-State Plasmonic Nanopores. Nano Lett. 2014; 14:6917–6925. [PubMed: 25347403]
66. Belkin M, Aksimentiev A. Molecular Dynamics Simulation of DNA Capture and Transport in Heated Nanopores. ACS Appl. Mater. Interfaces. 2016; 8:12599–12608. [PubMed: 26963065]
67. Piana S, Lindorff-Larsen K, Shaw DE. Atomic-Level Description of Ubiquitin Folding. Proc. Natl. Acad. Sci. U. S. A. 2013; 110:5915–20. [PubMed: 23503848]
68. Bhattacharya S, Yoo J, Aksimentiev A. Water Mediates Recognition of DNA Sequence *via* Ionic Current Blockade in a Biological Nanopore. ACS Nano. 2016; 10:4644–4651. [PubMed: 27054820]

69. Lucent D, Vishal V, Pande VS. Protein Folding under Confinement: A Role for Solvent. Proc. Natl. Acad. Sci. U. S. A. 2007; 104:10430–10434. [PubMed: 17563390]
70. Wei R, Gatterdam V, Wieneke R, Tampe R, Rant U. Stochastic Sensing of Proteins with Receptor-Modified Solid-State Nanopores. Nat. Nanotech. 2012; 7:257–263.
71. Belkin M, Chao S-H, Jonsson MP, Dekker C, Aksimentiev A. Plasmonic Nanopores for Trapping, Controlling Displacement, and Sequencing of DNA. ACS Nano. 2015; 9:10598–10611. [PubMed: 26401685]
72. Reiner JE, Robertson JWF, Burden DL, Burden LK, Balijepalli A, Kasianowicz JJ. Temperature Sculpting in Yoctoliter Volumes. J. Am. Chem. Soc. 2013; 135:3087–3094. [PubMed: 23347384]
73. Belkin M, Maffeo C, Wells DB, Aksimentiev A. Stretching and Controlled Motion of Single-Stranded DNA in Locally Heated Solid-State Nanopores. ACS Nano. 2013; 7:6816–6824. [PubMed: 23876013]
74. Pang Y, Gordon R. Optical Trapping of a Single Protein. Nano Lett. 2012; 12:402–406. [PubMed: 22171921]
75. Phillips JC, Braun R, Wang W, Gumbart J, Tajkhorshid E, Villa E, Chipot C, Skeel RD, Kale L, Schulten K. Scalable Molecular Dynamics with NAMD. J. Comput. Chem. 2005; 26:1781–1802. [PubMed: 16222654]
76. Vanommeslaeghe K, Hatcher E, Acharya C, Kundu S, Zhong S, Shim J, Darian E, Guvench O, Lopes P, Vorobyov I, MacKerell AD Jr. CHARMM General Force Field: A Force Field for Drug-Like Molecules Compatible with the CHARMM All-Atom Additive Biological Force Fields. J. Comput. Chem. 2010; 31:671–690. [PubMed: 19575467]
77. Yoo J, Aksimentiev A. Improved Parametrization of Li^+, Na^+, K^+, and Mg^{2+} Ions for All-Atom Molecular Dynamics Simulations of Nucleic Acid Systems. J. Phys. Chem. Lett. 2012; 3:45–50.
78. Andersen HC. Rattle - a Velocity Version of the Shake Algorithm for Molecular-Dynamics Calculations. J. Comput. Phys. 1983; 52:24–34.
79. Miyamoto S, Kollman PA. SETTLE: An Analytical Version of the SHAKE and RATTLE Algorithm for Rigid Water Molecules. J. Comput. Chem. 1992; 13:952–962.
80. Darden TA, York D, Pedersen L. Particle Mesh Ewald: An N log(N) Method for Ewald Sums in Large Systems. J. Chem. Phys. 1993; 98:10089–92.
81. Humphrey W, Dalke A, Schulten K. VMD: Visual Molecular Dynamics. J. Mol. Graphics. 1996; 14:33–38.
82. Martyna GJ, Tobias DJ, Klein ML. Constant Pressure Molecular Dynamics Algorithms. J. Chem. Phys. 1994; 101:4177–4189.

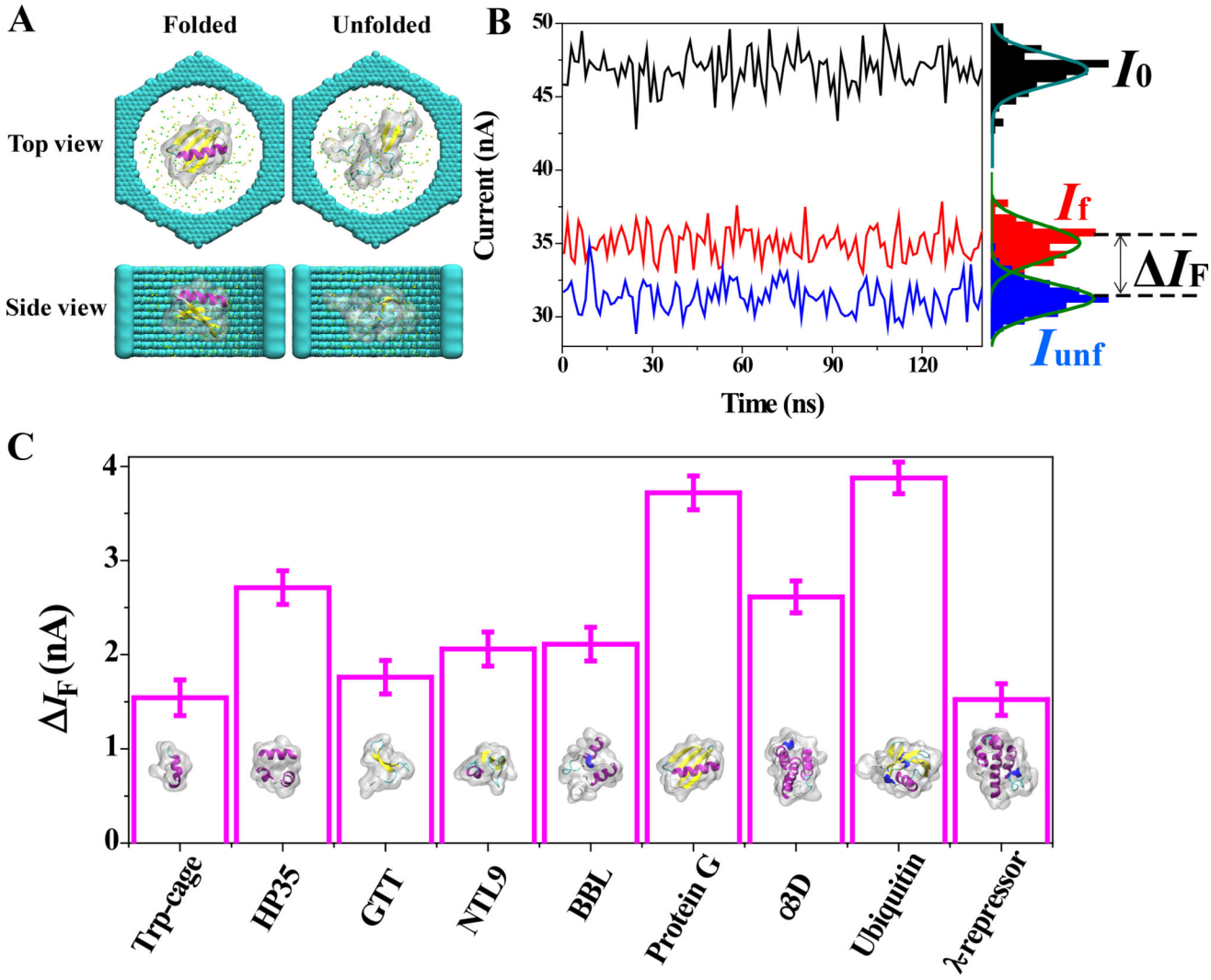

Figure 1.

Ionic current blockades report on the folding state of a protein. (A) A typical simulation system containing a folded (left) or unfolded (right) protein (protein G^{24}) at the center of a 6 nm-diameter solid-state nanochannel (cyan). An electric field is applied along the axis of the channel, the protein is restrained to maintain its initial conformation. The protein is colored according to the secondary structure of its folded conformation: purple indicates α-helix, yellow indicates β-sheet, white and cyan indicate coil and turn, respectively; the semitransparent molecular surface represents the excluded volume of the protein. Green and yellow spheres depict potassium and chloride ions, respectively; water is not shown for clarity. (B) Ionic current recorded from MD simulations of protein G placed in the nanopore in the folded (red) and unfolded (blue) states. The black trace indicates ionic current recorded in the absence of the protein. All-point histograms of the current values are shown at the right axis. The current traces were sampled every 2.4 ps and averaged in 1.2 ns blocks. The ionic current difference between the folded and unfolded states $\Delta I_F = I_f - I_{unf}$, where I_f and I_{unf} are the average currents in the folded and unfolded states, respectively. Data shown were obtained under applied electric field of 74.67 mV/nm; the concentration of the KCl

electrolyte was 2 M. (C) Blockade current difference (ΔI_F) for nine proteins. Inset images illustrate the folded conformations of the proteins. All other conditions as in panel B. The eight additional simulation systems are shown in SI Figure S1. Error bars represent the standard error of ΔI_F computed from the 150 ns ionic current traces averaged in 1.2 ns blocks.

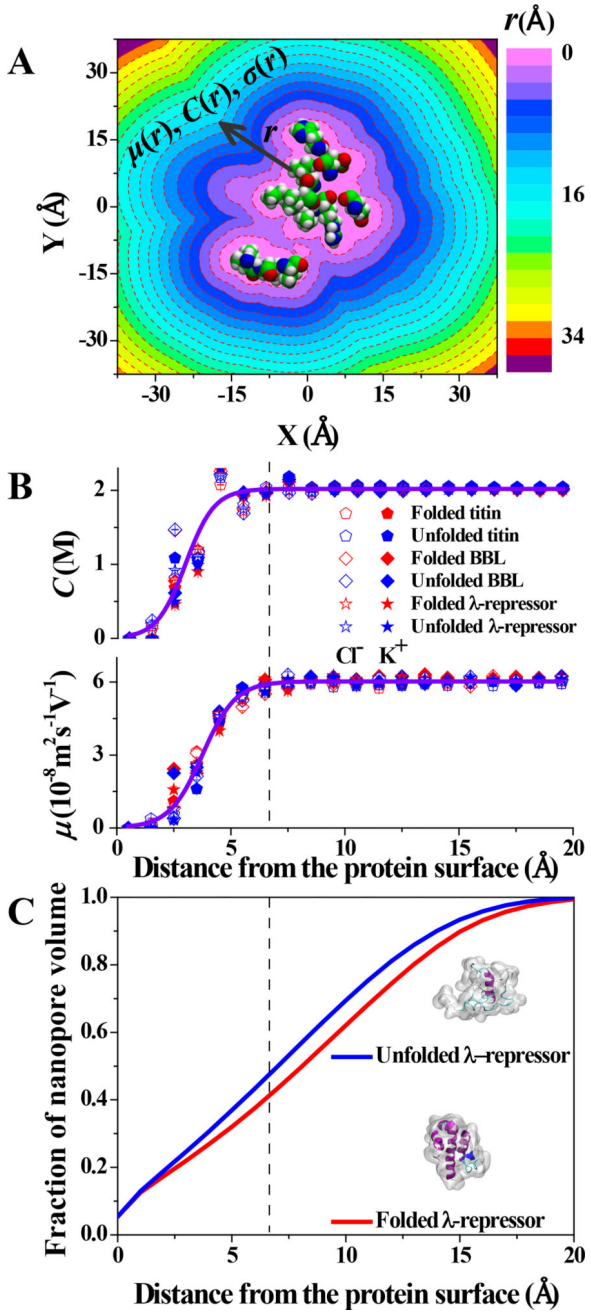

Figure 2.

Microscopic origin of the blockade current dependence on the folding state of a protein. (A) Cross section of a simulation system. Atoms of the protein are shown as vdW spheres (white, red, blue and green indicate hydrogen, oxygen, nitride and carbon atoms, respectively), the solvent is shown as a contour plot colored according to distance to the nearest protein surface, r. The ion concentration, $C(r)$, mobility, $\mu(r)$, and electrolyte conductivity, $\sigma(r)$, depend on the distance from the protein surface. (B) The average ion concentration (top) and ion mobility (bottom) *versus* distance from the protein surface for the folded and unfolded conformations of the following three proteins: titin (a 119-residue

monomer of the I27 domain), BBL (long peripheral subunit-binding domain) and λ-repressor. The data were obtained from 30 ns MD simulations of the positionally restrained proteins submerged in 2 M KCl electrolyte and subject to an electric field of 71.43 mV/nm. The data were averaged over all ions and all frames of the MD trajectories. Error bars (representing standard errors) are smaller than the symbols. (C) The fraction of the nanopore volume occupied by the protein and the solvent surrounding the protein within distance r of the protein surface as a function of r. The data are shown for folded and unfolded conformations of λ-repressor; SI Figure S3 shows data for all other proteins featured in Figure 1C. The dashed lines in panels B,C schematically indicate the distance $r^* = 6.6$ Å at which $C(r)$ and $\mu(r)$ attain their bulk values.

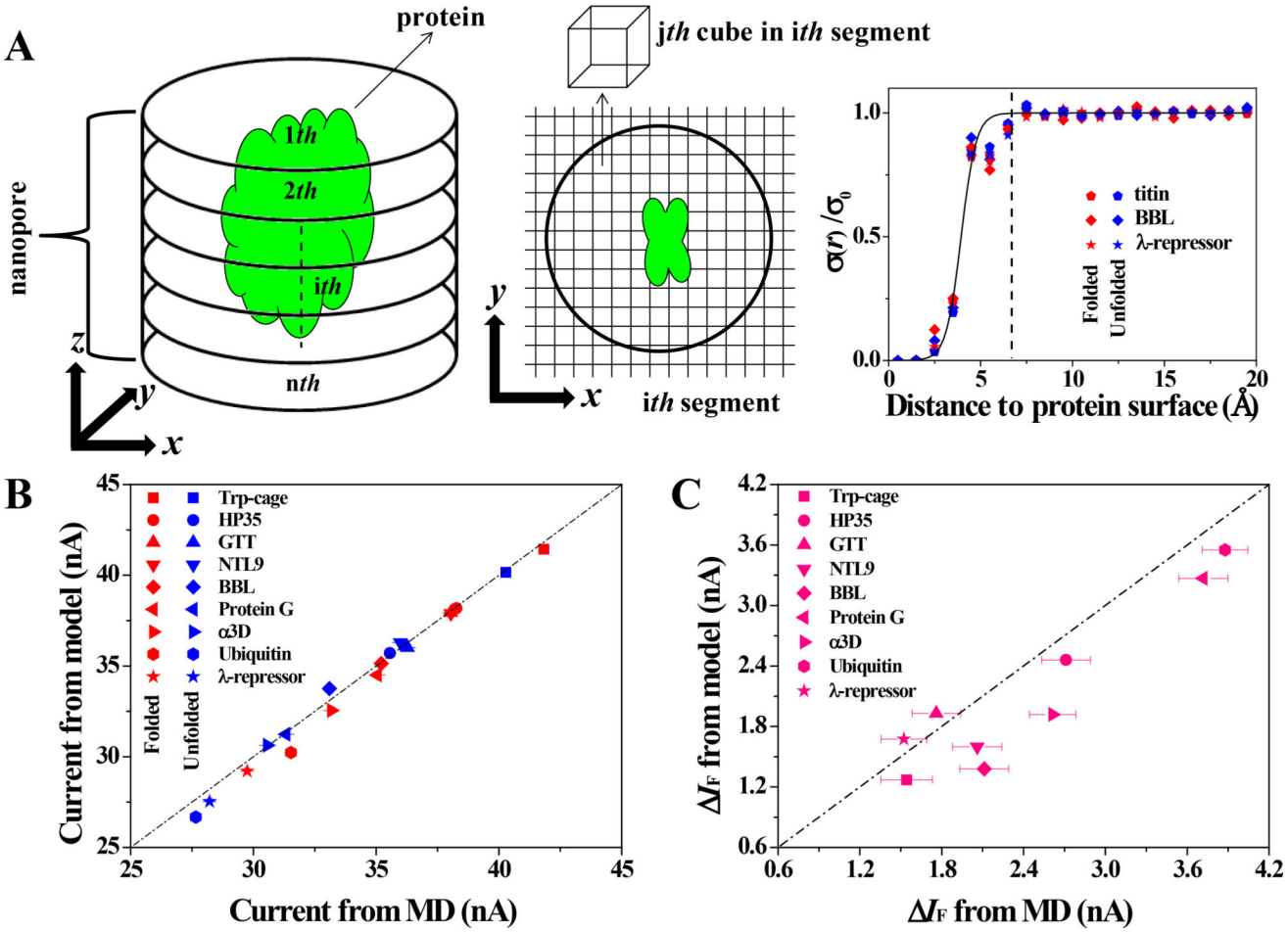

Figure 3.

Theoretical model of blockade current. (A) Schematic illustration of the model. The nanopore volume is represented by a cylinder split into n segments along the nanopore axis; the green object represents the volume of a protein. Each segment is further divided using a rectangular grid, such that the entire volume of the nanopore is represented by a collection of 1 Å^3 cubes. The conductivity of the electrolyte in each cube is calculated by first computing the distance of the cube's center to the nearest protein surface and then using the established dependence of the electrolyte mobility $\sigma(r)$ on the distance. The right panel shows $\sigma(r)$ normalized by the bulk conductivity, σ_0. (B) The nanopore current predicted by the model *versus* the nanopore current measured in MD simulations for nine proteins in folded and unfolded conformations. In all cases, an electric field of 74.67 mV/nm was applied along the nanopore axis, the KCl concentration was 2 M. The protein conformations used for the theoretical model calculations was the same as in the all-atom MD simulations of the ionic current. The dashed line indicates perfect agreement between model and simulation. Error bars represent standard errors. (C) Same as in panel B but for ΔI_F.

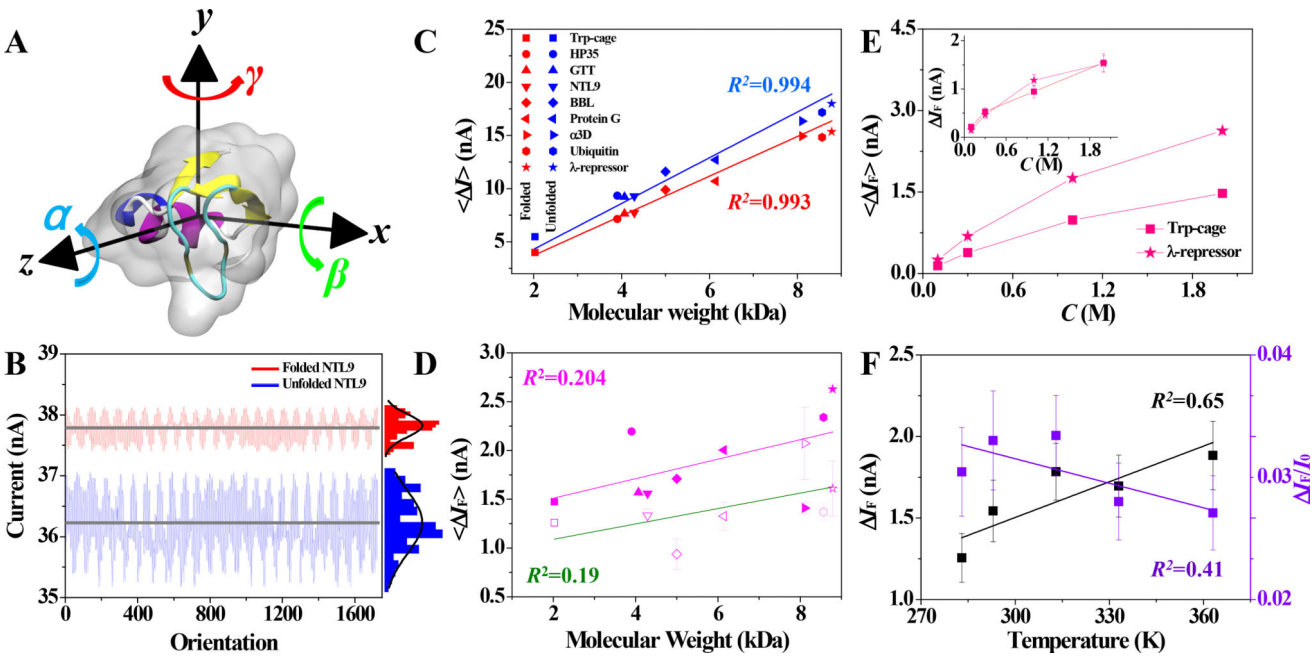

Figure 4.

The effect of protein orientation, ion concentration and temperature on the ionic current difference produced by protein folding. (A) Rotation angles α, β and γ that define protein orientation. (B) Blockade current, I, for 1728 unique orientations of the NTL9 protein in the folded and unfoded states. The ensemble of orientations was produced by changing angles α, β and γ in 30° increments. Horizontal lines indicate the rotation-averaged blockade currents. For each protein state, the plot also shows an all-point histogram of the currents (off the right axis) and its fit to a Gaussian distribution (black line). The blockade current was computed using a theoretical model featured in Figure 3. Data for eight other proteins are shown in SI Figure S6. (C) Rotation-averaged blockade current amplitude $< \Delta I > = I_0 - < I >$ *versus* molecular weight of the proteins. Rotation-averaged values were obtained using the theoretical model. Lines represent linear fits to the data. (D) The blockade current difference (ΔI_F) between the mean currents produced by the folded (I_f) and unfolded (I_{unf}) proteins. The mean currents were obtained from rotation-averaged values plotted in panel C (filled symbols) and analysis of protein folding trajectories (open symbols). Symbols are defined in panel C. Lines represent linear fits to the data. Error bars represent standard errors in determination of the mean blockade current difference $< \Delta I_F >$ produced by averaging over the conformational ensembles. (E) ΔI_F *versus* bulk electrolyte concentration. Data in the main plot represent rotation-averaged ΔI_F values computed using the theoretical model. The inset shows all-atom MD data for fixed-conformation proteins. (F) Temperature dependence of the blockade current difference (ΔI_F, left axis) and the relative blockade current difference ($\Delta I_F/I_0$, right axis). I_0 indicates the open pore current. Data shown were obtained from ~ 150 ns all-atom MD simulations of the Trp-cage protein for a single fixed conformation. Error bars represent standard errors of 1.2 ns block-averaged data. Lines illustrate linear fits to the data.

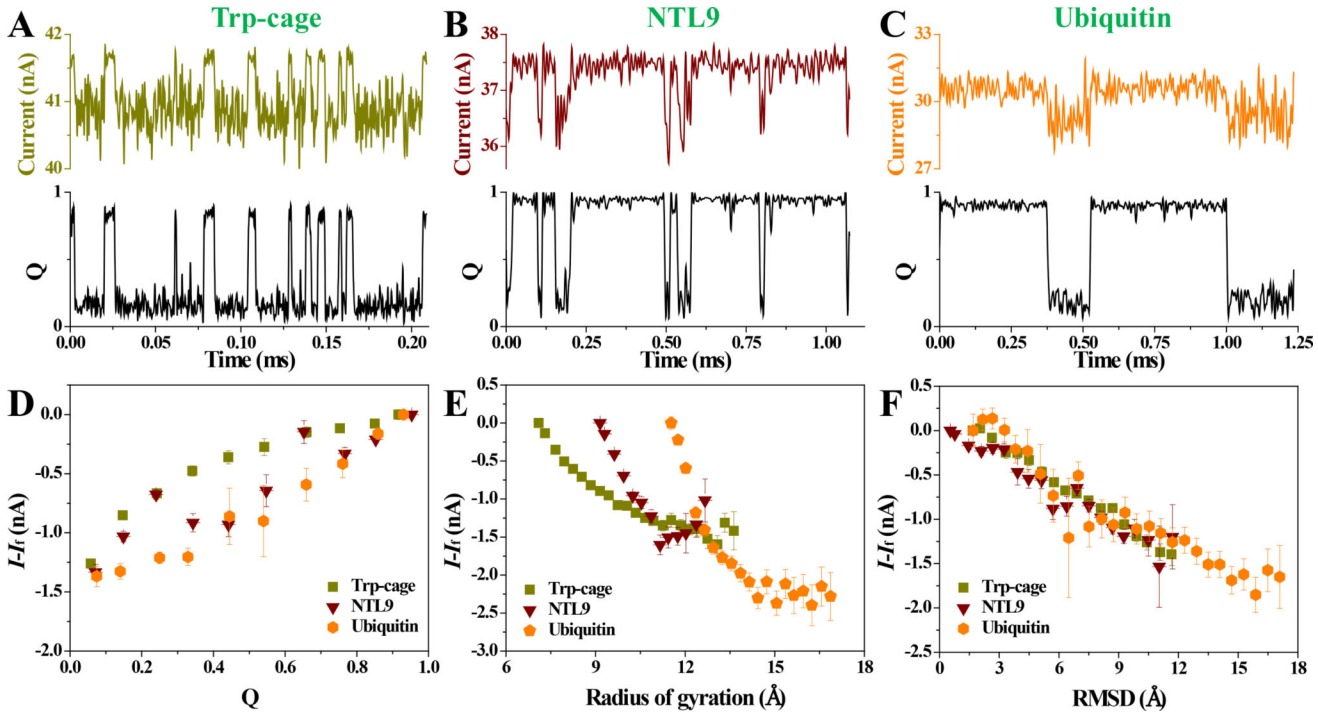

Figure 5.

Real-time detection of protein folding-unfolding transitions. (A–C) Simulated ionic current recordings from a single protein undergoing folding-unfolding transitions (top panels). The corresponding changes in the folding parameter Q is shown on the bottom panels. The ionic current recordings were obtained by applying the theoretical model of ionic current blockades (Figure 3) to millisecond all-atom protein folding trajectories reported by the D.E. Shaw group.[24,67] The traces shown for Trp-cage were sampled at 10 MHz and smoothed with a low-pass filter at 2 MHz. And the traces shown for NTL9 and ubiquitin shown were sampled at 1 MHz and smoothed with a low-pass filter at 200 kHz. (D–F) The average difference between the current blockades produced by a folding intermediate of that protein (I) and a fully folded protein (I_f). In panels D, E and F, the protein folding intermediates are categorized according to their Q values, radius of gyration and RMSD from the native folded states. Error bars represent standard errors.